Measurement Verification of Plane Wave Synthesis Technique Based on Multi-probe MIMO-OTA Setup

Wei Fan[1], Xavier Carreño[2], Jesper Ø. Nielsen [1] , Kim Olesen [1], Mikael B. Knudsen [2], Gert F. Pedersen[1]
[1] APNet, Department of Electronic Systems, Faculty of Engineering and Science, Aalborg University, DK-9220 Aalborg, Denmark {wfa, jni, ko, gfp}@es.aau.dk
[2] Intel Mobile Communications, DK 9220 Aalborg, Denmark {xavier.carreno, mikael.knudsen}@intel.com

***Abstract*—Standardization work for MIMO OTA testing methods is currently ongoing, where a multi-probe anechoic chamber based solution is an important candidate. In this paper, the probes located on an OTA ring are used to synthesize a plane wave field in the center of the OTA ring. This paper investigates the extent to which we can approach the synthesized plane wave in practical measurement systems. Both single plane wave with certain AoA and multiple plane waves with different AoAs and power weightings are synthesized and measured. Deviations of the measured plane wave and the simulated plane wave field are presented in terms of phase and power. Possible reasons for the deviations are also investigated.**

I. INTRODUCTION

Multiple Input Multiple Output (MIMO) technique has been one of the most attractive and promising methods to increase wireless system performance in terms of data throughput and reliability. New wireless technologies such as LTE, LTE-Advanced and WiMAX employ multiple antennas in mobile terminals.

In MIMO systems, both propagation channel conditions and antennas have significant impact on system performance. It is also important to take into consideration the interaction between MIMO devices and nearby objects, for instance, human hand and head. Too optimistic assumptions may lead to overestimation of the MIMO performance, and therefore testing of MIMO devices must be done under realistic conditions. The most realistic way to test MIMO devices is to test them as they are used in the final product, so-called MIMO Over-The-Air (OTA) testing. Standardization work for the development of the MIMO OTA test methods is currently ongoing. Several approaches were proposed and are under investigation. One of the candidates is the multi-probe anechoic chamber based method, which is considered as the most promising and technically advanced approach [1].

Often a radio channel can be considered as a collection of plane waves with different amplitude and phase weightings, Angle of Arrivals (AoAs) and polarizations, additionally taking into consideration other relevant channel parameters e.g. delay spread and Doppler spread, etc. For plane wave field synthesis with multiple probes in an anechoic chamber, the fundamental question is to which extent we can control the field structure inside the test zone where the device under test is located. Plane wave synthesis in the center of an OTA ring by use of multiple probes has been discussed in several contributions. In [2], the synthesis of the test zone fields was discussed based on spherical wave expansions. The power deviation of the synthesized field from the target field is studied for a varying number of OTA probes and for a varying size of the test zone for the different AoAs of the target plane wave field. Only the power deviation was selected to check the test zone behavior. Phase deviation over the test zone is equally important and even more critical to investigate.

In this paper, the multiple probes located on an OTA ring are used to synthesize plane wave fields in the center of the OTA ring. The plane wave fields are synthesized in a simple way where weighting of the OTA probes is based on the Least Square Error (LSE) optimization technique. This paper investigates to which extent we can approach the synthesized plane wave in practical measurement systems. Both single plane wave with certain AoA and multiple plane waves with different AoA and power weighting are synthesized and measured.

II. PLANE WAVE SYNTHESIS AND OPTIMIZATION

According to [2], as a rule of thumb, the relation between the required number of OTA antennas and the dimension of the test zone is:

$$K = 2\left\lceil \frac{\pi D}{\lambda} \right\rceil + 1 \qquad (1)$$

where K is the required number of probes, D is the diameter of the test zone, and λ is the wavelength. The square brackets round up the number inside the bracket to the nearest integer. In this study, synthesis of the plane wave field by use of 8 OTA probes is investigated. 0.7 wavelength is selected as the test zone diameter, which corresponds to approximately 8cm.

For a single plane wave synthesis case, the target plane wave field inside the test zone is assumed to be a field with uniform power distribution and ideal linear phase front along the impinging plane wave direction.

The target field vector $\mathbf{T}_{1\times M}$ contains the field for M sampled points inside the test zone. The element (i,j) in the transfer matrix $F_{K\times M}$ defines the propagation coefficient from the i-th OTA probe to the j-th sample point in the test zone, which is obtained from FDTD simulations [3]. Here K denotes the number of OTA probes. Then the weighting vector $\mathbf{G}^{Opt}_{1\times K}$ of the OTA probes is obtained using the LSE technique:

978-1-4673-1881-5/12/$31.00 ©2012 IEEE

$$\mathbf{G}_{1\times K}^{Opt} = \arg \min_{\mathbf{G}_{1\times K}} \left\| \mathbf{G}_{1\times K}\mathbf{F}_{K\times M} - \mathbf{T}_{1\times M} \right\| \quad (2)$$

For the multiple plane waves case, the target field is a coherent summation of the single plane waves,

$$\mathbf{T}_{total} = \sum_{i=1}^{N} P_{AoA}(i) \cdot \mathbf{T}(i) \quad (3)$$

where $P_{AoA}(i)$ is the power for the i-th single plane wave, $\mathbf{T}(i)$ is the target field of i-th single plane wave, which is calculated based on the AoA of the plane wave. The optimization procedure to calculate the weighting vector for multiple plane waves case is the same as in the single plane wave case.

The amplitude and phase for each probe in the measurement system are set according to the weighting vector G in a channel emulator, see below.

III. MEAUREMENT SYSTEM AND CALIBRATION

The measurement system configuration setup is illustrated in Figure 1. Power amplifiers (PA) are used to adjust power at the DUT to the required level.

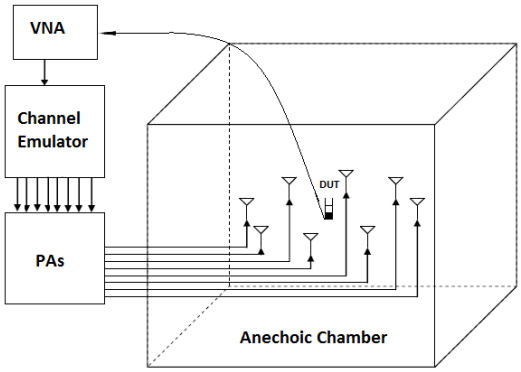

Figure 1. An illustration of the MIMO OTA test system in the measurement setup. The 8 probes are equally spaced on a circle around the test zone where the device under test (DUT) is located.

The measurement system consists of a VNA, an Elektrobit F8 channel emulator, an anechoic chamber, 8 horn antennas as OTA probes, a dipole antenna as DUT located in the center of the chamber, turntable that supports the DUT, cables and amplifiers. The measurements are carried out at 2.655GHz. For the current work, we consider only the case with vertical polarization.

Figure 2 shows the anechoic chamber setup in the measurement system. Wood masts have been used to support and fix the horn antennas. The wood masts are partially covered by absorbers to avoid reflections during the test (not shown in the figure). Polystyrene, which has a very low interaction with Electromagnetic (EM) waves, is placed on top of the turntable to support the DUT. The horn antenna characteristics are detailed in [3]. Only the upper OTA ring is used during the measurements.

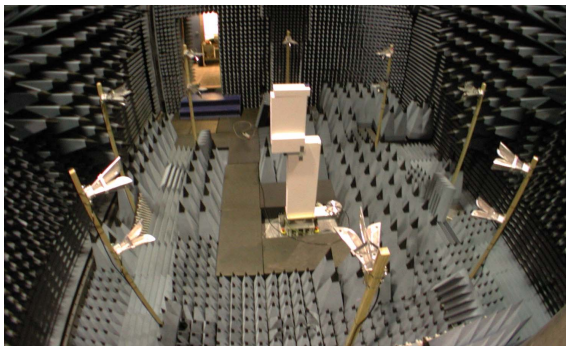

Figure 2. Setup used in the MIMO OTA testing.

Phase and amplitude calibrations are performed for each probe before the measurements. The goal of the calibration is to compensate errors caused by measurement setup non-idealities, i.e. probe placement and orientation error, etc. The target is that equal field response at the center can be obtained for all the probes.

In this paper, AoA of the plane wave is defined in the counter-clockwise direction and AoA 0 degrees is defined as the field arriving to the test zone from probe one as illustrated in Figure 3.

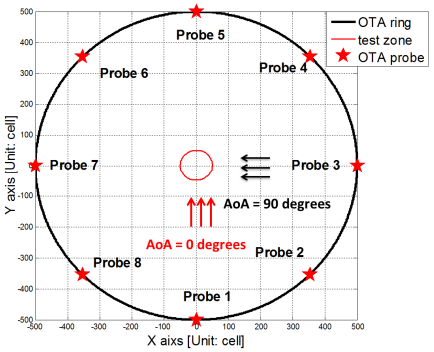

Figure 3. Illustation of OTA probe location and AoA of the plane wave field. Cell resolution is selected to be 0.005m in FDTD simulations

A. *Measurement scenarios*

In order to measure the field structure generated by plane wave synthesis technique, a dipole is fixed on the turntable and rotated on a circle with a fixed radius to the center at 0cm, 3cm, 6cm, and 9cm, respectively. The field structure inside the test zone, slightly outside the test zone and far outside the test zone, which corresponds to field structure at 3cm, 6cm, 9cm radius, will be investigated for different scenarios including single plane wave with certain AoA and multiple plane waves with different AoAs and power weightings.

As for the synthesis of a single plane wave field, ideal field has uniform power and linear phase front along the impinging wave direction inside the test zone. As the measurements are performed on the circle with radius 3cm, the phase variation curve along orientation of turntable should follow an ideal sinusoid curve. Field structure outside the test zone may present variations in power and phase due to fading.

While for the synthesis of multiple plane wave fields, field structure can present fading both inside and outside test zone.

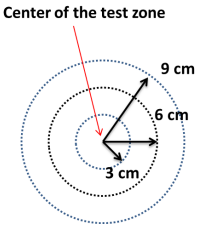

Figure 4. Illustration of the measurement diagram

Three scenarios are synthesized and measured. The details are listed in Table I. If the synthesized plane wave is arriving to the test zone from the direction where one of the OTA antennas are located, the test zone performance is expected to be the best since essentially only one relevant probe will synthesize the field. The worst case is the synthesis of a plane wave field impinging from an angle exactly in the middle of two adjacent OTA probes [5].

TABLE I CONSIDERED SCENARIOS DETAILS

Scenario name	Details
Scenario A	Single plane wave arrives to the test zone with AoA = 0 degrees
Scenario B	Single plane wave arrives to the test zone with AoA = 22.5 degrees
Scenario C	Two plane wave arrive to the test zone with AoA = 180 degrees and 85 degrees, respectively. The power for the two plane wave fields are the same.

The focus of this paper is the variations of the measured and simulated field over different orientations, so the measured power and phase are normalized to mean values.

B. Accuracy investigation of MIMO OTA setups

Before performing the measurements, the stability of the channel emulator and the anechoic chamber is investigated. If the signal can fluctuate over time due to instability, this will essentially affect the synthesized field. The impact of VNA used in the study is assumed to be negligible. In the stability study, the anechoic chamber is measured over 10 hours and maximum variations of 0.15dB and 1.6 degrees have been found with respect to signal power and phase variations, respectively. As for the channel emulator, stability studies have been performed over 10s and 10 hours for a single fader input-to-output link. For the short period, maximum variations of 0.2dB and 1.2 degrees have been found with respect to power and phase, respectively, while standard deviations of up to 0.6 dB and 6.4 degrees have been observed for the long period. The main reasons for the variations are likely the temperature change of the environment and the signal drifting inside the channel emulator over the time. Since the measurements are performed in a relatively short period for each scenario, we assume the impacts from instability of the anechoic chamber and channel emulator are negligible.

Ideally, the anechoic chamber should be totally silent, that is, reflections should be completely avoided inside the anechoic chamber. The reflections of the anechoic chamber are investigated before the measurements. A wideband horn antenna is located in the middle of the test zone and measurements are performed in frequency domain. The frequency domain data is transformed by an inverse FFT to yield a time domain signals. It was found that the largest reflection is 0.35m away from the main peak. The main peak corresponds to the line of sight (LOS) propagation, while the next peak corresponds to a reflection from the cable near the turntable. The largest reflection is at least 15 dB less than the maximum power level for all orientations of the horn antenna. The impact of reflections inside anechoic chamber can be considered as negligible.

The power coupling between probe antennas can also affect the synthesized field performance. In the measurements, OTA probe one is selected as the transmitted antenna and we measure the signal levels at the other probes. As illustrated in Figure 5, OTA probe 5, which is located on the boresight direction of probe one, presents the maximum coupling. At 2.655GHz, the maximum power coupling is less than -40dB, which will have negligible impact on the synthesized field structure.

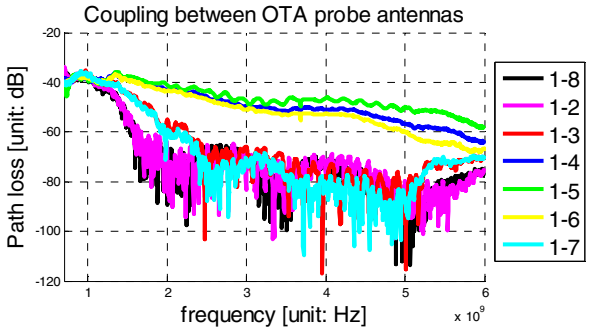

Figure 5. Couplings between OTA probe antennas, legend 1-*i* denotes the power couping between probe one and the *i*-th probe

IV. MEASUREMENT RESULTS

A. Errors at radius = 0cm

Ideally, when the test dipole is located in the center of the test area, the field structure should be constant over all orientations of the turntable. However, there are some factors that will contribute to inaccuracies of the measurements. The cables that connect the test dipole to the VNA are moving and bending around the turntable during the measurements. Also, although the center of the test zone and the OTA probe locations are set by use of a positioning laser, the placements of the OTA probes and the test dipoles may not be ideal. Apart from the location of the test dipole, asymmetric orientation of the test dipole may also affect the field structure. Impact of OTA probe antenna placement error including orientation error and location mismatch on the test zone field structure is investigated in detail in [5].

As illustrated in Figure 6, the phase variations over the orientation of the turntable approximately follow a sinusoid wave for all scenarios. For both scenario A and B, the maximum variation of phases is around 20 degrees, which corresponds to 0.62cm at the measurement frequency.

Considering the tendency of the phase variation curve, the dipole is located -0.31cm away from the ideal center along the propagation direction. As for scenario C, dipole is located 0.31cm away from the ideal center along the propagation direction. The ripples are likely generated by the cable bending. Statistics of phase and power variations at radius 0cm for all scenarios are listed in Table II.

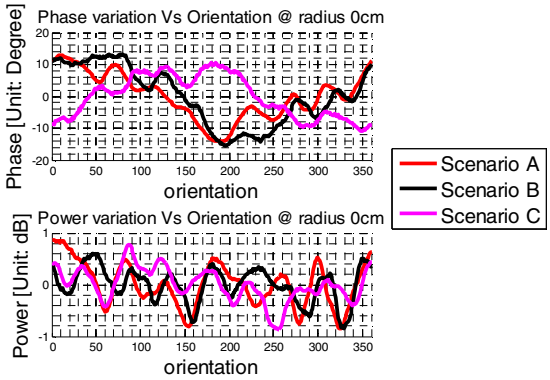

Figure 6. phase and power variations at radius 0cm for all scenarios

TABLE II PHASE AND POWER VARIATIONS AT RADIUS 0CM FOR ALL SCENARIOS

	STD (Phase deviation) [degree]	STD (Power deviation) [dB]
Scenario A	7.2	0.42
Scenario B	9.1	0.33
Scenario C	6.6	0.32

B. Comparison results for scenario A

As shown in Figure 7, measured phase variation matches quite well with the simulations, while the measured power variation also approximately follows the tendency of the simulated power. Statistics of power and phase deviations between the measurements and simulations for all radiuses in scenario A are listed in Table III. Compared with statistics of scenario A in Table II, similar error statistics have been found for measurements at radius 3cm and 6cm. As for 9cm measurements, phase deviations are much larger. As shown in Figure 8, one possible reason causing such deviations may be because the test dipole presents location error of around 0.6cm along the propagation direction of the field (which corresponds to 40 degrees maximum difference between the measurements and simulations).

TABLE III STATISTICS OF PHASE AND POWER DEVIATIONS FOR ALL RADIUSES IN SCENARIO A

	STD (Phase deviation) [degree]	STD (Power deviation) [dB]
3cm	6.92	0.34
6cm	8.99	0.37
9cm	17.29	0.41

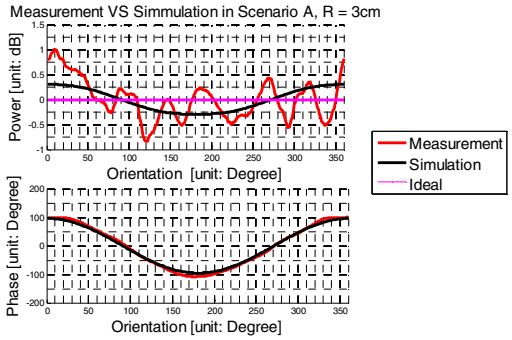

Figure 7. Simulation and measurement comparisions for single plane wave with AoA = 0 degrees in terms of power and phase variations at radius 3cm

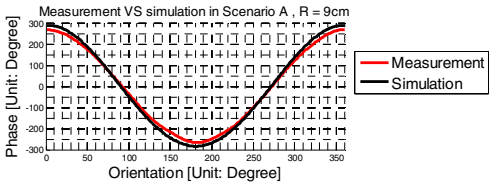

Figure 8. Simulation and measurement comparisions for single plane wave with AoA = 0 degrees in terms of phase variations at radius = 9cm

C. Comparision results for scenario B

As shown in Figure 9, good agreements have been achieved between the measurements and simulations with respect to both power and phase for scenario B with radius 6cm. Statistics of phase deviations and power variations for all radius in scenario B are listed in Table IV. Compared with statistics of scenario B in Table II, similar error statistics have been observed at radius 3cm and 6cm. As for the 9cm measurements, the deviations are large with respect to both phase and power. As shown in Figure 10, the simulated and measured fields don't fade at the same orientation angles and fading for the measurements are deeper. Phase jumping of π occurs when the signal is in deep fading. Also, phase measurement is quite inaccurate when the signals are in deep fade. It is a demanding request to have fading at the exact same orientations in practical measurement systems and the results are expected.

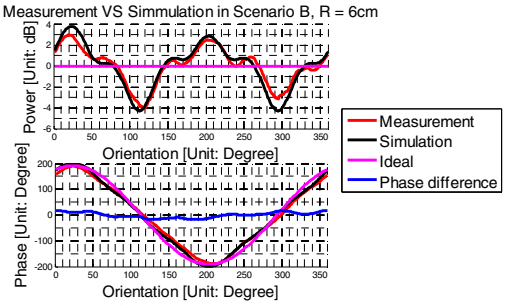

Figure 9. Simulation and measurement comparisions for single plane wave with AoA = 22.5 degrees in terms of power and phase variations

TABLE IV STATISTICS OF PHASE AND POWER DEVIATIONS FOR ALL RADIUSES IN SCENARIO B

	STD (Phase deviation) [degree]	STD (Power deviation) [dB]
3cm	7.31	0.42
6cm	10.69	0.59
9cm	53.10	5.09

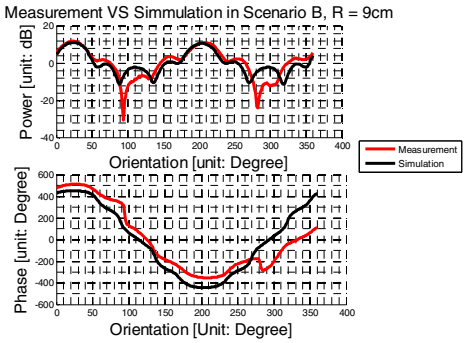

Figure 10. Simulation and measurement comparisions for single plane wave with AoA = 22.5 degrees in terms of power and phase variations at radius 9cm

D. Comparision results for scenario C

As shown in Figure 11, we can see similar tendency between the measurements and simulations with respect to power variations for scenario C with radius 6cm. As for the phase, phase jumping of π occurs when the signal is in deep fading. The fades are caused by the coherent superposition of two plane waves with different AoAs. The simulated and measured fields don't fade simultaneously and the fading for the measurements are deeper. Also, phase measurements are quite inaccurate when the signals are in fades. Those will contribute to large deviations between simulations and measurements. Statistics of phase deviations and power variations for all radiuses in scenario C are listed in Table V. Compared with statistics of scenario C in Table II, similar error statistics have been found for measurements at radius 3cm.

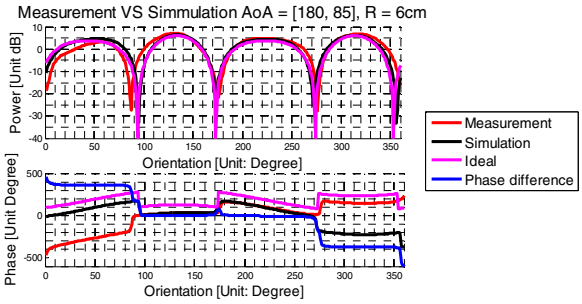

Figure 11. Simulation and measurement comparisions for two plane waves with same power and AoA 180 degrees and 85 degrees respectively in terms of power and phase variations.

TABLE V STATISTICS OF PHASE AND POWER DEVIATIONS FOR ALL RADIUSES IN SCENARIO C

	STD (Phase deviation) [degree]	**STD (Power deviation) [dB]**
3cm	6.39	3.12
6cm	40.41	4.84
9cm	25.47	3.07

However, the standard deviations with respect to phase and power deviations listed in Table V can be misleading. Due to the fact that fades don't occur at the exact same orientations, very large deviations can be observed in the transient region where fading takes place. As shown in Figure 13, large power deviations exist only in very small number of orientations. As for the phase deviations, deviations are generally larger due to the fact that phase measurements are not accurate when fades occur (As shown in Figure 12).

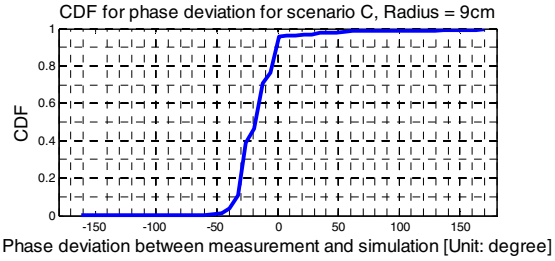

Figure 12. CDF of phase deviation for scenario C with radius 9cm.

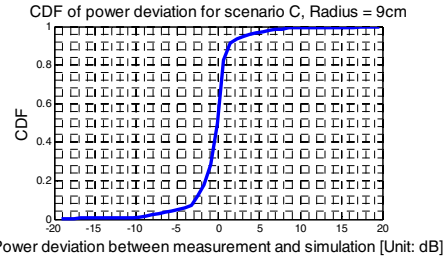

Figure 13. CDF of power deviation for scenario C with radius 9cm.

V. CONCLUSION

Good agreement between measurements and simulations has been achieved in terms of both phase and power inside the test zone area (radius = 3cm) for all scenarios.

Similar tendencies have been observed for the simulated and measured plane wave field with respect to both power and phase for all scenarios outside the test zone. However, with the presence of fading, deviations become large due to the fact that fading in simulations and measurements don't occur at the exact same orientations. Phase measurements are quite inaccurate when the signals are in deep fades.

Without the presence of fading, standard deviations of up to around 10 degrees and 0.6 dB have been found with respect to phase and power respectively. The following sources of inaccuracies have been identified: DUT placement error, cable effect such as bending, instruments impact.

REFERENCE

[1] Measurement of radiated performance MIMO and multi-antenna reception for HSPA and LTE terminals (Release 11) 3GPP TR 37.976 V1.5.0 (2011-05), R4-112505.

[2] T. A. Laitinen, P. Kyosti, J.-P. Nuutinen, and P. Vainikainen, "On the number of OTA antenna elements for plane-wave synthesis in a MIMO-OT A test system involving a circular antenna array," in The 4th European Conference on Antennas and Propagation (EuCAP'lO), Barcelona, Spain, Apr. 12-16, 2010.

[3] O. Franek, G. F. Pedersen, "Spherical Horn Array for WideBand Propagation Measurements," IEEE Transactions On Antennas And Propagation, 59, 2011 (7) p. 2654-2660.

[4] P. Kyösti, T. Jämsä, J-P Nuutinen, "Channel Modelling for Multiprobe Over-the-Air MIMO Testing", in International Journal of Antennas and Propagation, vol. 2012, (submitted).

[5] W.Fan, J. Nielsen, X. Carreno, M. Knudsen, G. Pedersen, "Impact of probe placement error on MIMO OTA test zone performance," IC1004 TD(12)03044, Feberary 2012.